Nonlinear Dynamic Analysis of Automotive Seat Rails: Experimental Insights for Enhanced Modal Testing Design

Philipp Wagner

Chair of Vibro-Acoustics of Vehicles and Machines, Department of Engineering Physics and Computation, TUM School of Engineering and Design, Technical University of Munich, Boltzmannstraße 15, Garching, 85748, Germany.
BMW Group, Knorrstrasse 147, Munich, 80937, Germany. E-mail: philipp.wa.wagner@bmw.de

Patrick Langer

BMW Group, Knorrstrasse 147, Munich, 80937, Germany.

Marcus Maeder and Steffen Marburg

Chair of Vibro-Acoustics of Vehicles and Machines, Department of Engineering Physics and Computation, TUM School of Engineering and Design, Technical University of Munich, Boltzmannstraße 15, Garching, 85748, Germany.

(Received 12 December 2025; accepted 3 May 2026)

The vehicle seat rail is a crucial connection between the passenger seats and the vehicle chassis, featuring complex adjustment mechanisms that result in intricate, nonlinear vibration behavior. Accurate characterization of these dynamics is essential for optimizing designs to meet noise, vibration, and harshness requirements. Traditional linear modal analysis methods are often inadequate in capturing amplitude-dependent behaviors, while nonlinear methods typically require extensive measurements and prior knowledge of the system's nonlinearities. This study employs an advanced experimental modal analysis that combines response- and force-controlled stepped-sine testing with harmonic force surface techniques. This approach extracts quasi-linearized frequency response functions, including amplitude and phase information, without prior assumptions about nonlinearity. A comprehensive measurement campaign, supported by computer tomography, investigates variability in bearing positions and their effects on vibration, quantifying key sources of uncertainty. The presented seat rail analysis demonstrates the possibilities and limitations of linear and nonlinear approaches for weakly nonlinear systems. It also provides practical recommendations for their appropriate application areas. These findings provide valuable insights into the dynamics of automotive seat rails and establish a practical experimental framework. Future work will enhance the accuracy of force identification and extend the method to more complex nonlinear systems, enabling better predictive modeling and design optimization.

1. INTRODUCTION

Automotive seat rails are complex structural dynamic systems essential to occupant safety and vehicle ride comfort. In the context of *noise, vibration, and harshness* (NVH), these components serve as the primary transfer path for vibrations propagating from the vehicle to the passenger. However, accurately characterizing the dynamic behavior of seat rails presents significant challenges due to their intricate designs, which feature adjustment mechanisms, cylindrical and roller bearings, and lightweight, thin-walled parts. Structural joints, widely used in automotive assemblies, such as seat rails, introduce significant nonlinearities and nonlinear damping mechanisms. These include dry friction and micro-slips, which can significantly impact NVH performance.

Research often focuses on specific design parameters to address various issues. In this context, Mazur et al.[1] investigated the sensitivity of seat rails to manufacturing variations. They found that ball size directly affects NVH behavior and the track's sensitivity to sliding efforts. Similarly, Yu et al.[2] studied the distribution of gaps in seat rail joints under uncertain structural parameters. They determined that increasing preload can reduce abnormal noise caused by gaps between the inner and outer rails. As a solution, they proposed an optimized preload value that balances noise reduction with functionality. Furthermore, Zhang et al.[3] characterized seat vibration behavior and found that rattle noise strongly correlates with specific low-frequency structural modes, particularly the seat frame's torsion mode. However, a significant limitation of these studies is the difficulty of applying traditional linear modal analysis to systems dominated by strong nonlinearities.

Contrary to linear systems, nonlinear mechanical systems exhibit response-amplitude-dependent stiffness and damping. Allemang and Avitabile[4] and Lin et al.[5] comprehensively elaborate on these effects. Additionally, Brake et al.[6] highlight that joints introduce localized nonlinearities primarily influenced by friction and contact mechanics. As noted by Islam et al.[7]

and Nestrovic et al.,[8] these factors complicate the accurate identification of modal parameters using standard experimental modal analysis. Consequently, conventional linear modal analysis methods offered by commercial tools often fail to accurately identify modal parameters in the presence of nonlinearities, as the superposition principle is invalid.

To address this challenge, Rosenberg[9] introduced the concept of *nonlinear normal modes* (NNMs), which represent the in-phase vibrations of a conservative system. Building on Rosenberg's work, Kerschen et al.[10–12] showed that the NNMs of the underlying conservative system function as attractors for the trajectories of the damped system. This allows for the practical computation of frequency-energy plots that characterize amplitude-dependent frequencies and bifurcations. Furthermore, Goncalves[13] and Piqueira et al.[14] addressed the limitations of Rosenberg's synchronous assumption and provided a robust mathematical framework for analyzing general damped nonlinear systems. Bridging theory and practice, Szemplińska-Stupnicka[15] proposed the *single nonlinear resonant mode* (SNM) theory, demonstrating that a single nonlinear mode can effectively approximate near-resonant responses by a single NNM. This theoretical framework enhanced the experimental investigation. Peeters et al.[16] made significant advancements by extending the classical phase-resonance method to nonlinear systems. By maintaining a 90-degree phase lag between the excitation and the response, they successfully isolated a single NNM in experimental settings, enabling them to extract amplitude-dependent frequencies and damping ratios.

Building on these modal concepts, researchers have since explored methods to directly extract nonlinear parameters from frequency response data. In this context, Gibert[17] developed methodologies for fitting measured response curves to nonlinear modal models. Recently, advancements in experimental techniques have enabled better isolation of nonlinear modes. Significant contributions to the field include the work of Ehrhardt and Allen et al.,[18] as well as Kwarta and Allen et al.[19] These researchers developed a new algorithm that employs multi-harmonic excitation signals to identify the backbone curves of nonlinear normal modes in nonlinear structures. This method facilitates the reconstruction of the near-resonance response using a single nonlinear resonant-mode model, as described in the previously mentioned paper.[15]

Additionally, Scheel et al.[20,21] expanded phase-resonance testing to strongly damped systems. However, recent research indicates that under specific testing conditions, particularly when the response amplitude is kept constant, these systems can exhibit quasi-linear behavior. This quasi-linearization enables the extraction of amplitude-dependent modal parameters using standard linear identification techniques.

Moreover, the field of nonlinear modal analysis has been significantly enhanced by the contributions of Kuran and Özgüven.[22] They developed a modal superposition method to analyze the forced harmonic response of nonlinear structures. Their work provides a framework for understanding the effect of nonlinearities on system dynamics, offering a basis for further methodological advancements. Arslan et al.[23] focus on parametric identification of structural nonlinearities using measured frequency response data. This method enables a detailed analysis of the impact of nonlinearities on modal parameters, providing valuable insights into the intricate nature of nonlinear systems.

To address these identification challenges, Karaağaçlı et al.[24] proposed the *response-controlled stepped-sine* testing (RCT) and the *harmonic force surfaces* (HFS) concept to accurately identify the modal properties of nonlinear mechanical systems with multiple discrete nonlinearities. Later, they extended the RCT-HFS framework[25] to address mechanical systems with continuously distributed nonlinearities. Both works demonstrated the framework's efficacy in systems with significant conservative nonlinearities and low-to-moderate damping. Subsequently, they further developed the RCT-HFS approach in the paper[26] and the patent EP4078113[27] for accurate modal identification of non-conservative mechanical systems exhibiting friction-induced high nonlinear damping by utilizing the concept of complex nonlinear modes. The response-controlled stepped-sine testing method represents a paradigm shift by demonstrating that most nonlinear mechanical systems exhibit almost (quasi)-linear behavior, maintaining a constant displacement amplitude at the driving point during stepped-sine testing.[24–26] This control strategy forces the system into a quasi-linear state, even in the presence of strong nonlinearities that typically cause bifurcations in standard force-controlled testing methods. This discovery enabled the accurate identification of response-level-dependent modal parameters of various strongly nonlinear mechanical systems by applying standard linear modal analysis techniques to quasi-linear frequency response functions (FRFs) measured via a response-controlled stepped-sine test. In the works,[24–26] the HFS concept primarily served as a validation tool for evaluating the accuracy of nonlinear modal parameters identified by RCT. Furthermore, Karaağaçlı et al.[28] comprehensively investigated the backbone curve identification of the harmonic force surfaces.

Previous studies[24–26,28] indicate that the standard procedure in the RCT-HFS framework involves constructing harmonic force surfaces from harmonic force spectra measured at different constant displacement amplitudes. Once this is conducted, constant-force FRFs can be extracted by intersecting the harmonic force surfaces at constant-force levels. Finally, these frequency response functions are compared with those synthesized from nonlinear modal parameters identified through RCT. However, during the nonlinear experimental modal analysis of miniature piezo-actuators, Karaağaçlı et al.[29] proposed an alternative approach to constructing the HFS. They propose building the harmonic force surfaces from response spectra measured at constant force levels instead. To extract constant-response FRFs, they recommended intersecting the HFS with constant-response planes. In their study, the constant-response frequency response functions were found to be quasi-linear, as expected, and processed to derive response-level-dependent nonlinear modal parameters. Later, Gürbüz et al.[30] demonstrated the effectiveness of this procedure for the nonlinear modal identification of a beam assembly with a bolted-lap joint.

In this study, the HFS-RCT framework is applied to automotive seat rails, utilizing its unique ability to address the complex, friction-dominated nonlinearities identified by Mazur,

Yu, and Tatari. This approach provides a methodology for experimentally analyzing amplitude-dependent vibration behavior and addressing existing challenges in predicting NVH performance in seating systems. Furthermore, this investigation advances previous studies by precisely extracting phase information from the linearized transfer functions. While this study demonstrates the suitability and effectiveness of the presented HFS method, it acknowledges that challenges remain. These include the sensitivity of force identification to measurement errors and the method's applicability. The analysis offers practical recommendations for effectively using the harmonic force surfaces concept and addresses existing gaps in current research. In conclusion, this work provides valuable experimental insights for automotive engineers, enhancing their understanding of amplitude-dependent behaviors essential for optimizing various NVH design requirements.

The work is organized as follows: First, the theoretical foundations necessary for the experimental application are presented. Subsequently, an overview of the measurement setup and the relevant boundary conditions is provided. The fourth section evaluates measurement uncertainties and assesses the methodology's effectiveness in analyzing nonlinear behavior. Section five will validate this approach and discuss its limitations. Finally, the main conclusions are summarized, and the focus for future research is outlined.

2. THEORETICAL BACKGROUND

This work investigates the nonlinear structural dynamic behavior of seat rails using modal analysis techniques. For this purpose, the RCT-HFS approach enables the effective investigation of vibrational characteristics. To ensure completeness, the theoretical derivations of this framework provided in[24] are summarized below.

In general, the dynamics of a discrete system with n degrees of freedom is expressed as a second-order differential equation:

$$\mathbf{M}\,\ddot{\mathbf{u}} + \mathbf{C}\,\dot{\mathbf{u}} + \mathbf{K}\,\mathbf{u} + \mathbf{f}_{\mathrm{nl}}(\mathbf{u}, \dot{\mathbf{u}}) = \mathbf{f}; \tag{1}$$

where $\mathbf{M} \in \mathbb{R}^{n\times n}$ denotes the discrete system mass matrix. The linear terms of the damping $\mathbf{C} \in \mathbb{R}^{n\times n}$ and stiffness matrices $\mathbf{K} \in \mathbb{R}^{n\times n}$ are derived using the small disturbance calculation approach.[31] The displacements are represented by the column vector $\mathbf{u} \in \mathbb{R}^n$. Furthermore, $\mathbf{f}_{\mathrm{nl}}$ describes the nonlinear discrete internal forces, which generally depend on the displacements $\mathbf{u}$ and velocities $\dot{\mathbf{u}} \in \mathbb{R}^n$. All external forces acting on the system are represented by $\mathbf{f} \in \mathbb{R}^n$.

The following discussion assumes a structure that is excited harmonically and exhibits viscous, proportional damping[a]. By utilizing the exponential approach $\mathbf{u}(t) = \mathrm{Re}\{\bar{\mathbf{u}}\mathrm{e}^{\mathrm{j}\omega t}\}$,[32] Eq. (1) is expressed in the frequency domain as:

$$\left(-\omega^2\mathbf{M} + \mathrm{j}\omega\mathbf{C} + \mathbf{K}\right)\bar{\mathbf{u}} + \bar{\mathbf{f}}_{\mathrm{nl}} = \bar{\mathbf{f}}. \tag{2}$$

In Eq. (2), ω represents the circular frequency and j the imaginary unit. The complex vectors $\bar{\mathbf{u}}$ indicate the displacement amplitudes, while $\bar{\mathbf{f}}_{\mathrm{nl}}$ denotes the nonlinear internal force amplitudes, and $\bar{\mathbf{f}}$ signifies the external force amplitudes. The term within the parentheses represents the linear dynamic stiffness matrix $\mathbf{Z}(\omega)$. Consequently, Eq. (2) separates the linear and nonlinear terms. This work employs an approach based on the *describing function method*[24,33] to accurately describe the amplitudes of internal nonlinear forces as the product of a so-called *nonlinearity matrix*[34] and the displacement vector:

$$\mathbf{f}_{\mathrm{nl}} = \Delta(\bar{\mathbf{u}})\,\bar{\mathbf{u}}. \tag{3}$$

In this context, $\Delta(\bar{\mathbf{u}}) = \mathrm{Re}\{\Delta(\bar{\mathbf{u}})\} + \mathrm{j}\,\mathrm{Im}\{\Delta(\bar{\mathbf{u}})\} \in \mathbb{C}$ defines the nonlinearity matrix, which is a complex, symmetrical, displacement-dependent nonlinear matrix. The real part of the nonlinearity matrix represents the conservative component and corresponds to an equivalent stiffness. Conversely, the imaginary term corresponds to the dissipative part and can be interpreted as equivalent damping. The equations can also be extended to accommodate multi-harmonic displacements, addressing symmetrical and asymmetrical nonlinearities. Karaağaçlı et al.[24] highlight the relation between the classical *harmonic balance method* (HBM) and the describing function method, which are used to analyze nonlinear systems subjected to harmonic excitation. Mathematically, these two approaches remain equivalent. However, the primary distinction lies in their representation of nonlinear internal forces. HBM uses a single force vector derived from a Fourier series, whereas the describing function method expresses these forces as the product of a nonlinearity matrix and a displacement-amplitude vector. Considering only the real part of the nonlinearity matrix, Eq. (2) becomes:

$$\left(-\omega^2\mathbf{M} + \mathrm{j}\omega\mathbf{C} + (\mathbf{K} + \mathrm{Re}\{\Delta(\bar{\mathbf{u}})\})\right)\bar{\mathbf{u}} = \bar{\mathbf{f}}. \tag{4}$$

The equation reveals that nonlinearity can be interpreted as a modified stiffness matrix $\tilde{\mathbf{K}} = \mathbf{K} + \Delta(\bar{\mathbf{u}})$. The term in the parentheses represents the dynamic stiffness of the nonlinear (modified) system $\mathbf{Z}(\omega, \bar{\mathbf{u}})$ as a function of displacement amplitude and frequency. Furthermore, if nonlinearity is an inherent component characteristic, such that the total number of degrees of freedom remains unchanged, this process is called *structural modification*. In contrast, when a nonlinear structure is connected to the system according to Eq. (4) and increases the number of degrees of freedom, this process is called *structural coupling*. This distinction is especially relevant in the context of dynamic substructuring.[34] To determine the nonlinear vibration modes, the nonlinear undamped eigenvalue problem of the following form is solved:

$$\left(\tilde{\mathbf{K}} - \omega_k^2(\bar{\eta}_k)\,\mathbf{M}\right)\,\tilde{\varphi}_k^{\mathrm{NNM}}(\bar{\eta}_k) = \mathbf{0}. \tag{5}$$

In this formula, $\tilde{\varphi}_k^{\mathrm{NNM}}$ explains the k-th real nonlinear normal modes along with their associated natural (circular) frequencies ω_k. Both variables depend on the k-th modal amplitude $\bar{\eta}_k$. In large systems, iterative solutions, such as the Newton-Raphson method,[35] can be highly computationally intensive. In these cases, the response-dependent nonlinear normal mode method,[36] which utilizes a dual-mode space that involves a second modal transformation, can significantly reduce the system size. The system discussed in Section 3 has 48 degrees of freedom and can still be effectively analyzed using the approach outlined in this section. In the following, it is assumed

[a]The assumption of viscous and proportional damping is not mandatory for treating the systems presented here and is used only for simplicity.

that the modes are well separated without any internal resonances. As a result, the normal modes remain relatively unchanged with varying amplitudes. Under this assumption, the near-resonance displacement can be transformed into modal space using *single nonlinear mode theory*:[15,24,35]

$$\bar{\mathbf{u}} = \tilde{\mathbf{\Phi}}^{\mathrm{NNM}}(\bar{\eta})\,\bar{\eta}. \tag{6}$$

The concept involves a single-point stepped-sine excitation applied at the driving point or any other arbitrary location. At this point, the displacement amplitude $\bar{\mathbf{u}}_1$ is maintained at a constant level, ensuring that $\bar{\mathbf{u}}_2, ..., \bar{\mathbf{u}}_n$ remains constant. However, the modal amplitude remains unchanged. As a result, knowing the number, type, or position of any nonlinearities present in the system is unnecessary. This is the fundamental principle of the response-controlled stepped-sine testing method.[24] Consequently, this methodology allows for the acquisition of quasi-linear frequency response functions. Therefore, Eq. (4) can be expressed in modal coordinates using the relationship from Eq. (6), followed by pre-multiplication with the transposed nonlinear modal matrix $\left(\tilde{\mathbf{\Phi}}^{\mathrm{NNM}}\right)^T$:

$$\left(-\omega^2\mathbf{M}_\eta(\bar{\eta}) + \mathrm{j}\omega\mathbf{C}_\eta(\bar{\eta}) + \mathbf{K}_\eta(\bar{\eta})\right)\bar{\eta} = \tilde{\mathbf{f}}(\bar{\eta}). \tag{7}$$

In Eq. (7), $\mathbf{M}_\eta(\bar{\eta})$ represents the modal mass matrix, $\mathbf{C}_\eta(\bar{\eta})$ denotes the modal damping matrix, and $\mathbf{K}_\eta(\bar{\eta})$ describes the modal stiffness matrix, with:

$$\begin{cases} \mathbf{M}_\eta(\bar{\eta}) = (\tilde{\mathbf{\Phi}}^{\mathrm{NNM}}(\bar{\eta}))^T\,\mathbf{M}\,\tilde{\mathbf{\Phi}}^{\mathrm{NNM}}(\bar{\eta}); \\ \mathbf{C}_\eta(\bar{\eta}) = (\tilde{\mathbf{\Phi}}^{\mathrm{NNM}}(\bar{\eta}))^T\,\mathbf{C}\,\tilde{\mathbf{\Phi}}^{\mathrm{NNM}}(\bar{\eta}); \\ \mathbf{K}_\eta(\bar{\eta}) = (\tilde{\mathbf{\Phi}}^{\mathrm{NNM}}(\bar{\eta}))^T\,\tilde{\mathbf{K}}\,\tilde{\mathbf{\Phi}}^{\mathrm{NNM}}(\bar{\eta}). \end{cases} \tag{8}$$

For external forces, the condition $\tilde{\mathbf{f}}(\bar{\eta}) = (\tilde{\mathbf{\Phi}}^{\mathrm{NNM}}(\bar{\eta}))^T\,\bar{\mathbf{f}}$ applies accordingly. In Eq. (7), the expression within the brackets represents the nonlinear stiffness matrix $\mathbf{Z}(\omega, \bar{\eta})$ in the modal domain. Thus, the following relation obtains for the modal amplitudes:

$$\bar{\eta} = \mathbf{Y}(\omega, \bar{\eta})\,\tilde{\mathbf{f}}; \tag{9}$$

with the admittance matrix, which relates to the inverse of the nonlinear stiffness matrix $\mathbf{Y}(\omega, \bar{\eta}) = \mathbf{Z}^{-1}(\omega, \bar{\eta})$ in the modal domain. The reverse transformation provides the displacement amplitudes in the following format:

$$\begin{aligned} \bar{\mathbf{u}} &= \mathbf{\Phi}^{\mathrm{NNM}}\,\mathbf{Y}(\omega, \bar{\eta})\,\tilde{\mathbf{f}} \\ &= \frac{\mathbf{\Phi}^{\mathrm{NNM}}\,(\mathbf{\Phi}^{\mathrm{NNM}})^T}{-\omega^2\mathbf{M}_\eta + \mathrm{j}\omega\mathbf{C}_\eta + \mathbf{K}_\eta}\,\bar{\mathbf{f}}. \end{aligned} \tag{10}$$

In the final step, the nonlinear normal modes are mass-normalized:

$$\mathbf{\Phi}^{\mathrm{NNM}} = \tilde{\mathbf{\Phi}}^{\mathrm{NNM}}\,\mathbf{M}_\eta^{-1/2} \Rightarrow \varphi_k^{\mathrm{NNM}} = \frac{\tilde{\varphi}_k^{\mathrm{NNM}}}{\sqrt{\mu_k}}; \tag{11}$$

$$2\delta = \mathbf{M}_\eta^{-1}\mathbf{C}_\eta; \quad \mathbf{\Omega}^2 = \mathbf{M}_\eta^{-1}\mathbf{K}_\eta; \tag{12}$$

with μ_k modal mass of the k-th mode. Hence, the FRF between the response point i and the excitation point r around the resonance region of the k-th mode can be expressed as follows:

$$\frac{\bar{\mathbf{u}}_i}{\bar{\mathbf{f}}_r} = \frac{\mathbf{\Phi}_{ik}^{\mathrm{NNM}}(\bar{\eta}_k)(\mathbf{\Phi}_{rk}^{\mathrm{NNM}}(\bar{\eta}_k))^T}{\Omega_k^2(\bar{\eta}_k) - \omega^2 + \mathrm{j}2\delta_k(\bar{\eta}_k)\omega} = \bar{\mathbf{Y}}_{ir}(\omega, \bar{\eta}_k). \tag{13}$$

Examining Eq. (13) reveals that all modal parameters depend on the modal amplitudes. Therefore, if the modal amplitude is kept constant, Eq. (13) is expected to yield a quasi-linear FRF. This forms the fundamental hypothesis of the SNM theory.[15] Numerous authors[24–26,29] have confirmed this hypothesis within the RCT-HFS framework across various experimental applications in nonlinear mechanical systems. This is achieved by maintaining the excitation point's displacement amplitude constant in a closed-loop control system. In this context, Eq. (13) has been successfully employed to identify response-level-dependent nonlinear modal parameters by fitting the equation to quasi-linear FRFs measured under constant response conditions using RCT. Furthermore, Eq. (13) facilitates the synthesis of constant-force FRFs by using response-dependent nonlinear parameters and a Newton-Raphson iterative solution method.[24] Consequently, the accuracy of the identified nonlinear modal parameters can be evaluated by comparing the synthesized frequency response functions with those experimentally obtained from the harmonic force surfaces, as discussed in Section 5.

3. MEASUREMENT SETUP

To implement the theoretical approaches discussed in Section 2, specific requirements for the test setup are necessary, which are outlined in this section. First, the measurement uncertainties associated with the adjustment mechanism are examined. For this purpose, the seat rail is moved from its initial position and then returned to a position midway between the upper and lower rails. After each adjustment, the center position is measured and evaluated[b]. Additional measurements are performed in the initial positions to obtain a meaningful number of measurements for uncertainty quantification. Second, the nonlinearity of the resulting vibration behavior is quantified. The analysis is based on the framework used in literature.[29,30]

Figure 1 illustrates the measurement setup utilized in this study. A high sensor resolution is employed to effectively capture global vibrations and local effects, allowing for the investigation of, for example, reciprocities between the upper and lower rails as initial indicators of nonlinear behavior. The analysis utilizes 16 sensors of type 354C03 from PCB PIEZOTRONICS, which offer a broad dynamic range of 100 mV/g to ensure a sufficient signal-to-noise ratio at low excitation amplitudes while preventing overloading at high excitation levels. A Tira GmbH type TV S 51120 shaker generates the necessary excitation amplitudes. Force and displacement control are managed using the commercial software Test.Lab from Siemens-LMS. The control is based on the impedance sensor of type 288D01 from PCB PIEZOTRONICS at the excitation point, the so-called driving point. The purpose of

[b] A comprehensive analysis of the seat rail position's impact on NVH behavior exceeds the scope of this work.

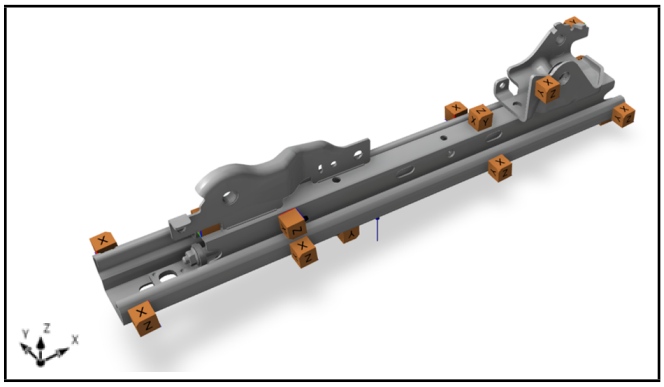

Figure 1. Representation of the measurement setup consisting of 16 tri-axis accelerometers and a shaker excitation in the y- and z-directions for the excitation of the torsional and the bending mode under free boundary conditions.

force-controlled excitation is to evaluate the structure's response/sensitivity to a constant force applied at different frequencies. The excitation energy level varies with frequency due to the system dynamics. A constant force amplitude in linear systems leads to a predictable response amplitude. However, the structure's response may depend on the excitation amplitude for nonlinear systems. A force-controlled sweep can reveal the jump phenomenon, where the response amplitude suddenly increases or decreases at specific frequencies.[34] These bifurcations occur because the system's effective stiffness and damping properties vary with the amplitude of the force.[36,37]

In contrast, during response-controlled stepped sine testing, the displacement amplitude at the excitation point is held constant (relative to the maximum displacement) across different frequencies, while the required force amplitude is varied. Maintaining a constant displacement amplitude stabilizes the system's energy level near resonance, allowing nonlinear effects to manifest at this specific amplitude.[24,38] Despite these circumstances, the frequency response appears more linear, yielding a quasi-linear transfer function even from nonlinear systems.

As previously mentioned, the response vibration behavior varies in force-controlled measurements. This can lead to significant changes in vibration behavior and unstable branches, even with very small frequency steps. The response-controlled stepped-sine test addresses this issue by maintaining a constant displacement amplitude. This approach yields a smooth response spectrum that includes points on the unstable branch.[24] Consequently, harmonic force spectra at various constant-displacement amplitudes will be recorded. These spectra can then be used to construct the harmonic force surface via linear interpolation between the individual measurements. The frequency response curve, which includes the unstable branches, can be determined by intersecting the measured quasi-linear FRFs at constant harmonic force levels using the HFS. However, based on the results in Section 4, the procedure reverses in this context. As suggested in literature,[29,30] the harmonic force surface is initially constructed from frequency response curves measured at various constant-force amplitudes. Quasi-linear frequency response functions are then obtained by intersecting the HFS along constant-displacement amplitude planes. Finally, these quasi-linear FRFs are processed with standard linear modal analysis techniques, such as peak-picking, to identify response-level-dependent nonlinear modal parameters.

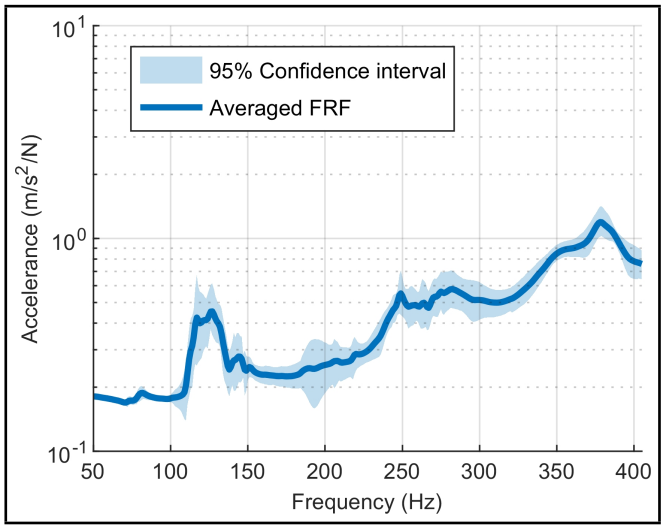

Figure 2. Representation of measurement uncertainties of the resulting FRF sum in the initial position, after varying the upper rail, represented as the mean value across all measurements and the 95 % confidence interval.

The excitation forces vary between 2 N and 30 N throughout this work. Under real loading conditions, forces of up to approximately 15 N would be sufficient. However, higher forces are applied to determine whether the modal parameters and frequencies converge. The force levels are also applied randomly to reduce viscoelastic damping effects, using linearly increasing excitation steps, and to emphasize the load-dependency factor. Furthermore, a stepped sine wave ranging from 50 Hz to 400 Hz is used as an excitation signal. Additionally, sufficient averaging is applied to reach a steady state and identify the first four dominant modes relevant to the overall configuration of the vehicle seat structure.

The seat rail is tested under free boundary conditions to prevent potential nonlinear effects arising from its attachment to the test dynamometer via bolts. This approach also aims to achieve better results in the higher frequency range. For this purpose, the rail is suspended at the seat frame connections using very soft elastic bands, keeping rigid-body vibrations at a frequency well below the first elastic mode. The boundary condition is assessed using the phase information from the driving point frequency response function, which must be between 0 and 180 degrees. Despite this requirement, the shaker's stinger provides some fixation. This setup is designed to handle high forces while minimizing lateral forces.

4. EXPERIMENTAL INVESTIGATION

The theoretical relationships can be explored experimentally using the special measurement setup described in Section 3. However, due to the nonlinear behavior, significant measurement uncertainties often arise.[6] Therefore, the first step is to determine the variance in the central position, which plays a crucial role in the design process.

4.1. Uncertainty Quantification

To evaluate repeatability, the upper rail is adjusted to various positions along its length. After each adjustment, the initial position is measured again, yielding 10 recordings. In the

next step, the FRF sum is computed over all sensor positions and directions, capturing the number of system changes. These FRFs facilitate uncertainty quantification, allowing for calculating mean values and 95 % confidence intervals, which are then visualized in Fig. 2.

The figure indicates that the reproducibility is sufficiently good before the first resonance at ca. 126 Hz and above 325 Hz. However, the wide confidence intervals in the first-resonance and medium-frequency ranges suggest that the variability of individual measurements significantly increases in amplitude and frequency. Specifically, the frequency of the first resonance becomes indeterminate and can vary by more than 10 Hz. The frequency corresponds to the system's first global torsional mode. The mode shape remains unchanged regardless of frequency shifts.

Non-destructive computer tomography is used to examine the seat rail and analyze the causes of low reproducibility. Figure 3 illustrates the various cylinder and ball bearings and the complex contact interactions between the upper and lower rails. This imaging technique precisely determines the positions of the bearings before and after adjustment.

The computer tomography analysis reveals that individual bearings can deviate from their initial positions, leading to nonlinear changes in contact areas that subsequently influence vibration behavior. Therefore, it is essential to know the adjustment history to accurately estimate the structural dynamic behavior. Alternatively, imaging techniques such as computer tomography provide precise bearing positions, thereby enhancing understanding and enabling comparisons with finite element simulations. Additionally, manufacturing-related pre-loads from overpressing the balls affect vibration behavior.[1] Consequently, this study employs the response-controlled stepped-sine testing to facilitate system analysis without requiring prior knowledge of the specific causes of nonlinearity.

4.2. Amplitude Dependent Behavior Analysis

The degree of nonlinearity is examined in the first step, explicitly screening for jump phenomena, as presented by Karaağaçlı and Özgüven.[24] For this purpose, the frequency range is analyzed with a constant sinusoidal signal, progressing from low to high frequencies. The sweep is then operated in the opposite direction. The results for a specific frequency range and two different excitation levels show that the curves exhibit only minor deviations within the typical measurement uncertainties. As a result, the seat rail does not show any significant bifurcations, indicating that the nonlinearity is relatively weak (Fig. 4). For weak nonlinearities, the HFS can be constructed from frequency responses measured at constant-force amplitude levels, as suggested in literature.[29,30] This eliminates the need for additional measurements when the displacement amplitude is constant. This approach significantly reduces the experimental effort.

Furthermore, the figure shows a notable decrease in the resonance frequency with increasing excitation amplitude, indicating softening behavior. This means that the resonance frequencies shift to lower values.[17,19] Following these observations, the next step is to conduct force-controlled stepped-sine measurements.

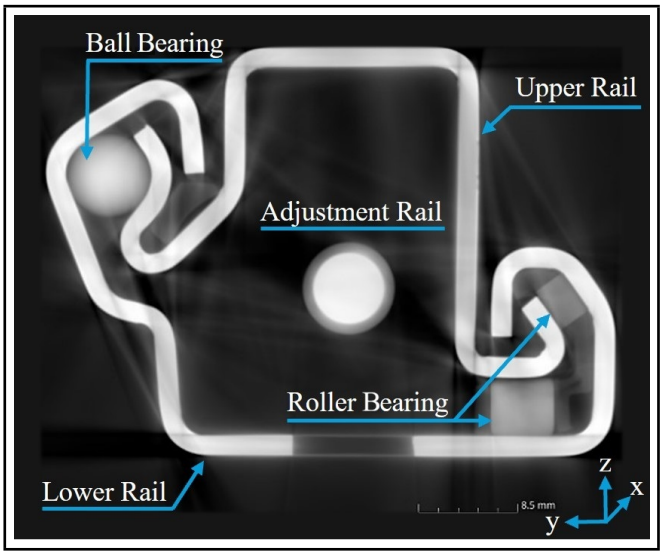

Figure 3. Non-destructive cause analysis using computer tomography of the seat rail, conducted before and after adjustment of the top rail, to determine the positions of the individual bearings.

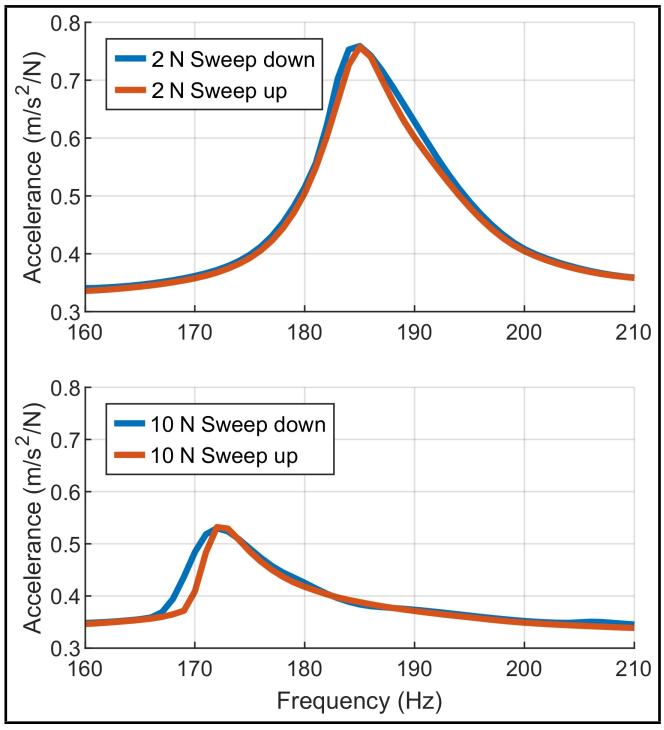

Figure 4. Energetic FRF Sum of all sensors for excitation of the seat rail in z-direction with sweep-up and sweep-down measurements at 2 N (top) and 10 N (bottom) to identify jump phenomena in the frequency range around the second resonance.

Figure 5 illustrates the transfer function summed across all measured sensors and directions for the respective excitation amplitudes presented in Section 3 over the entire frequency range. This figure highlights the first six dominant resonance frequencies relevant to the assembled seat configuration. These resonances occur at sufficiently different frequencies, as required by the single nonlinear resonant mode model presented in Section 2. The natural modes are determined and classified using the experimental modal analysis based on the PolyMAX algorithm.

Table 1 provides an overview of the individual eigenmodes. Due to the complexity of the combined motions, the designa-

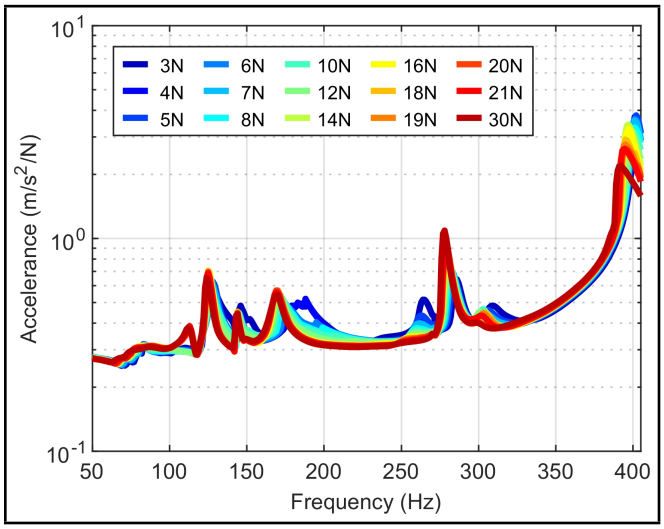

Figure 5. FRF Sum of all sensors for excitation in z-direction with different force amplitudes in the frequency range between 50 Hz and 400 Hz.

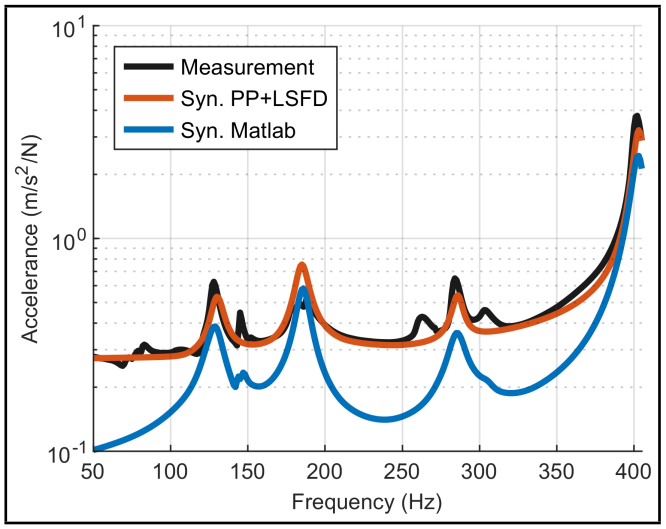

Figure 6. Comparison of the measured FRF Sum with the synthesized FRF Sum, based on peak-picking using the implemented least-squares frequency-domain (LSDF) algorithm and the MATLAB *modalfit* function, for identification at the lowest force level.

Table 1. The first six identified mode shapes and natural frequencies in Hz of the seat rail at an excitation amplitude level of 2 N in the z-direction, with a frequency range between 50 Hz and 400 Hz.

1	2	3	4	5	6
T_x^{1st}	$B_{y,\mathrm{rear}}$	$B_{y,\mathrm{front}}$	$B_{z,\mathrm{front}}$	$B_{z,\mathrm{rear}}$	T_x^{2nd}
126	185	259	281	305	400

tions refer to the components' respective dominant vibration behavior. Here, T_x^{1st} denotes the first torsional mode along the x-axis, while $B_{y,\mathrm{rear}}$ signifies the first bending mode around the y-axis, primarily influenced by the rear part of the rail.

Furthermore, the figure shows that all modes exhibit a softening behavior with increasing excitation. However, the behavior of the respective resonance is very inhomogeneous. In particular, a cancellation effect occurs at resonances between 240 Hz and 340 Hz. The resonances at 259 Hz and 305 Hz disappear with increasing excitation amplitude, so only the resonance at 281 Hz remains, performing a combined vibration from the other two. Consequently, the investigation focuses only on the four resonances at 126, 185, 281, and 400 Hz. The amplitude of the FRFs' first and third resonance frequencies increases with increasing excitation. In contrast, the second and fourth resonance frequencies show the opposite behavior with increasing damping. Therefore, the second resonance frequency is analyzed first, showing the most significant frequency shift. Accordingly, this resonance is best suited for evaluating the method's effectiveness and accuracy. Furthermore, the technique is subsequently applied to the other resonance frequencies.

Moreover, the data presented in Table 1 indicates that no vibration modes occur specifically in the x-direction within the frequency range being analyzed. Consequently, the number of spectra requiring linearization can be reduced from 48 to 32. This pre-selection supports reproducible identification of stable poles using linear methods by focusing solely on spectra that exhibit significant dynamics within the relevant frequency range.

4.3. Quasi-Linearization Process

The RCT-HFS method uses a master-slave approach to determine amplitude-dependent, quasi-linear frequency response functions. This methodology enables the conversion of conventional force-controlled frequency responses into spectra with constant displacements. Therefore, selecting an appropriate master channel is essential for a successful application based on force-controlled measurements. As shown in Table 1, the dominant modes are either torsion along the lateral axis or local bending in the front or rear regions. Thus, the driving point sensor, located at the shaker excitation position, is unsuitable as a master channel. Therefore, the first step is to identify a measurement channel that best captures the dominant vibration behavior across all resonances. For this purpose, this work employs the *optimal driving point* (OPD) criterion proposed by Imamovic and Ewins.[38,39] To evaluate the OPD, an experimental modal analysis is first conducted at the lowest force level, applying the approach presented in Section 4.4. It is assumed that the system behaves mainly linearly at this excitation level.

Furthermore, this initial modal identification is performed based on the measured acceleration FRF. This ensures that the method used here, which is based on peak-picking, does not identify false peaks across the full frequency range due to the $1/\omega^2$ decay per decade of the receptance. The result of this process is shown in Fig. 6.

The diagram displays the effectiveness of the employed method, which successfully captures the four resonances and accurately synthesizes the measured frequency response function. In contrast, the synthesis of the FRF using the MATLAB *modalfit* function, which relies on the same FRFs along with natural frequencies derived from the peak-picking method as initial values, reveals a distinct difference between the two approaches. This discrepancy arises primarily from the consideration of the lower and upper residuals during the modal parameter estimation process using the *least-squares frequency-domain algorithm* (LSDF). The method applies a least-squares approach to calculate the residuals. This approach focuses solely on the residuals to develop a physics-based model on the

Table 2. Results of the optimal driving point (OPD) criteria and the unit maximum component normalized mode shape values $|\Psi_r(j)|$ for the driving point (DP), the channel front left in z-direction (FL), the channel rear left in z-direction (RL), and the channel front right in z-direction (FR).

Ch	OPD	$\lvert\Psi_1(j)\rvert$	$\lvert\Psi_2(j)\rvert$	$\lvert\Psi_3(j)\rvert$	$\lvert\Psi_4(j)\rvert$
DP	0.03	0.07	0.01	0.04	0.02
FL	0.48	0.95	0.13	0.95	0.44
RL	0.43	0.78	1.00	0.25	0.17
FR	0.39	1.00	0.03	1.00	0.81

previously identified natural frequencies, damping ratios, and modal amplitudes. Therefore, Fig. 6 highlights the importance of considering out-of-band modes to achieve high-quality FRF synthesis. As a result of the modal identification process, the mode shapes required for the optimal driving point criterion can be determined. The results for the driving point and the top three channels with the highest OPD values are summarized in Table 2.

The table shows that, with a value of 0.03, the driving point sensor is not suitable as the master channel for the HFS extraction process. Furthermore, identifying a measurement channel that adequately captures all modes presents challenges. Therefore, the point located at the rear left in the z-direction, with an OPD value of 0.43, is selected, as it effectively represents the second mode, which is elaborated first.

Furthermore, the HFS is constructed as a continuous surface from harmonic displacement spectra for various force amplitudes, as shown in Fig. 7a. For this process, it is essential to create a smooth HFS curve to avoid undesirable effects such as *waviness* and *ruggedness*.[25] For this purpose, a Savitzky-Golay filter[40] is applied only to the master channel. In this context, the measured FRFs are used and integrated twice to compute the receptance, rather than using the measured displacement spectra directly. This approach offers several advantages.

First, the receptance can be transformed into the dynamic stiffness, which is already in polynomial form $(\mathbf{K} - \omega^2\mathbf{M})$. Hence, polynomial-based filters such as the Savitzky-Golay filter are particularly suitable. Additionally, the resonance peaks, which are essential for determining the damping ratio, are preserved while simultaneously reducing noise around them.[41] Since the back-and-forth inversion relies solely on the master channel, it involves only one vector from the FRF matrix, minimizing numerical effects. When determining nonlinear parameters, the real and imaginary parts of the dynamic stiffness correspond to the equivalent nonlinear stiffness and damping, allowing for separate filtering of these components.[28]

Moreover, it is advantageous to calculate displacement spectra from measured FRFs rather than using those generated by the measurement software. Usually, FRFs, which capture the system's characteristics and have a defined phase reference, are processed using an H1 or Hv estimator.[41] This processing reduces measurement noise. Additionally, via denormalization by multiplying by the measured shaker force spectrum, the resulting displacement spectrum has the same amplitude level and the same physical fluctuations (force drops) as the directly generated displacement spectra, while providing cleaner signals.

An additional significant challenge in applying the HFS

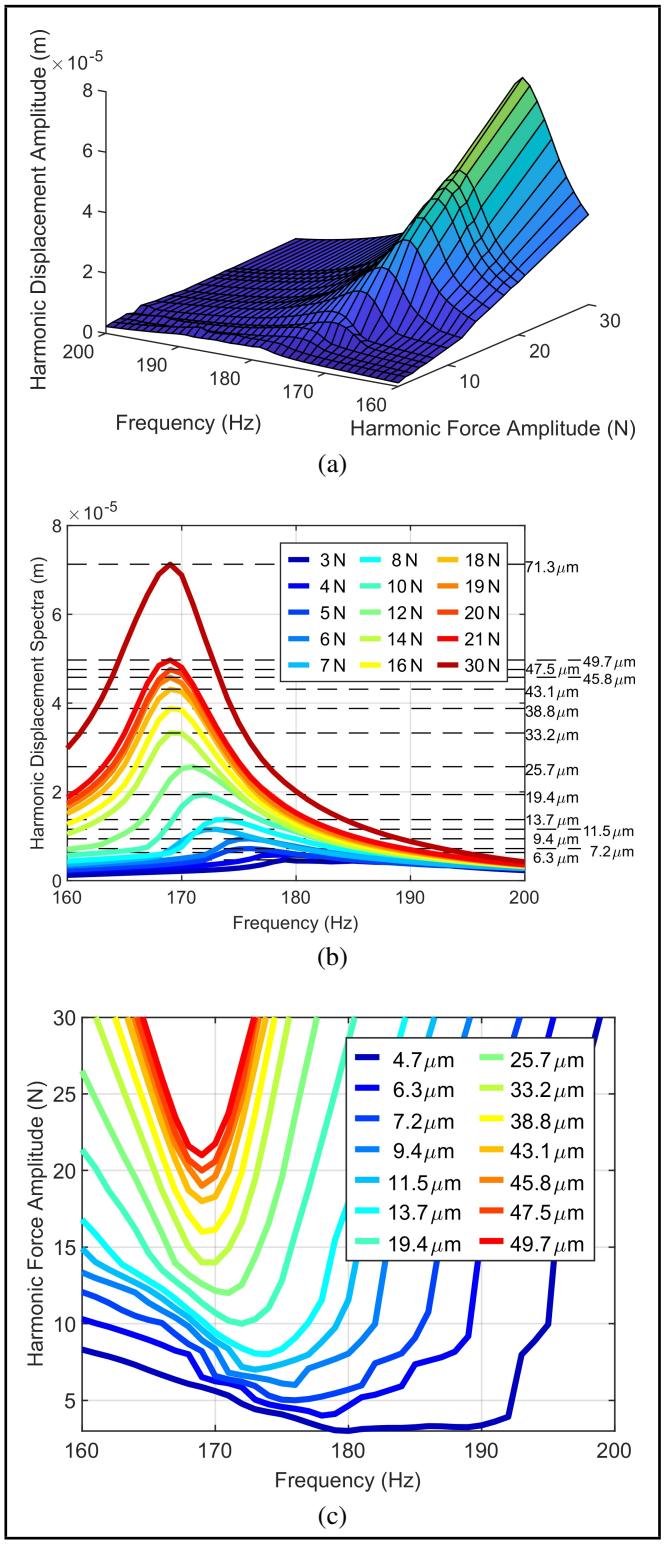

Figure 7. Quasi-linearization steps in the harmonic force surface (HFS) approach for weakly nonlinear systems using force-controlled stepped-sine measurements only: (a) harmonic force surface derived from displacement spectra across excitation forces at a representative sensor position; (b) harmonic displacement spectra across the various excitation levels, with cutting plans at the maximum of the spectra; (c) harmonic force spectra at the maximum of the constant displacement intersections of the HFS.

method arises from its reliance on the number of measurements. Increasing the number of sampling points yields a more accurate harmonic force surface interpolation. However, the intersection-plane process causes quasi-linear FRFs to exhibit broad peaks, particularly at lower displacement amplitudes, as

shown in Fig. 7c. These broad peaks result in an overestimation of damping ratios, leading to incorrect modal amplitudes. Consequently, out-of-band residuals are also overestimated due to the least-squares process, with errors propagating into the subsequent Newton-Raphson synthesis. To mitigate this issue, the lowest force level has been eliminated from the HFS computation. The removal of these additional sampling points is acceptable compared to the significantly improved stability of harmonic force surface extraction at the remaining displacement levels. However, 10 to 15 measurements are generally sufficient to achieve satisfactory results while limiting measurement effort.[24] Another approach could involve utilizing the damping value from the initial modal identification process during the optimal master channel determination step, which is conducted within an assumed range of linear behavior.

In the next step, the absolute maximum displacement, which represents the linearization point, is extracted across the entire reduced frequency band for each discrete excitation level. The geometric interpretation of this intersection is that by establishing a horizontal intersection plane through the three-dimensional HFS topography at its maximum amplitude, the system retains its maximum vibrational energy.[27] This level aligns precisely with the resonance peak of the respective sweep shown in Fig. 7b. The projection of this isoline provides a precise force profile necessary to maintain the desired target amplitude. Furthermore, the resulting V-shaped force spectrum reflects a physical limitation of the system. As frequency increases, the frequency band for a constant-amplitude signal gradually narrows. The underlying cause of this phenomenon lies in the dynamic stiffness matrix, which significantly increases away from resonance. To maintain constant displacement along the resonance slopes, significantly higher forces are typically required. This demand exceeds the shaker's physical power limit,[24,38] resulting in a reduction in the amount of usable measurement data within the examined frequency bands.[30] Determining the modal parameters poses significant challenges due to insufficient frequency and amplitude data. As a result, the truncated FRFs create an ill-conditioned least-squares problem during the LSFD process. To address this aspect, the boundaries are extended under the assumption that, in a classical RCT measurement, the shaker would adjust the force across the entire frequency range to maintain $\eta_k = \text{const}$. Consequently, the extracted forces are extended continuously and approximately linearly. Additionally, it is assumed that any nonlinearity at the boundaries is only weakly pronounced. Furthermore, outliers are removed after the extrapolation process.

The vibration responses of the remaining measurement channels, designated as slave channels, are evaluated to determine their complex displacements from the calculated force profile. For each frequency point, the slave channel's displacement is separately interpolated into its real and imaginary components, using the extracted force levels as interpolation points. This Cartesian decomposition method effectively avoids phase-wrapping discontinuities that could occur with a polar (magnitude and phase) interpolation approach.[38] Additionally, for the slave channels, the force profile is constrained to the range $[F_{min}, F_{max}]$ at the boundaries, preventing the displacement interpolation from extrapolating beyond the measured force range. This approach differs from that of the master channel, where complex boundary repetition strictly enforces a constant displacement amplitude.

Moreover, the HFS intersection encounters challenges due to topographical ambiguities. Contours generated from discrete data points, along with measurement noise, can sometimes lead to small, closed-loop shapes. In the context of highly nonlinear structural dynamics, such isolated circular shapes are known as isolas, which have resonance branches disconnected from the main branch.[10–12] These isolas are classified as measurement artifacts and are typically eliminated in favor of a continuous backbone curve, highlighting a methodological limitation. The traditional sweep method is inadequate for investigating these phenomena, necessitating advanced control techniques such as phase-locked loops (PLLs) or control-based continuation methods. For more information, see references.[20,42–44] To avoid misclassifying isolas as measurement uncertainties, additional measurements are performed with a frequency range up to 5 kHz and an excitation at the first resonance frequency, focusing on identifying the dominant higher harmonics of the fundamental frequency, detailed in Table 1. The analysis revealed an amplitude difference of greater 20 dB between the higher harmonics and the fundamental frequency. Therefore, it is assumed that the identified isolas were artifacts resulting from the geometric intersection of the HFS. These artifacts were subsequently filtered from the force spectra for further analysis. Such issues particularly arise at lower force amplitudes or with high modal density.

Finally, to generate quasi-linear FRFs, an element-by-element complex division is performed.[45] This approach reveals a crucial methodological implication: at the peak of the HFS topography, only a single discrete frequency and amplitude point exists. Consequently, the necessary resonance slopes for this highest energy level are absent. This limitation indicates that only $n - 1$ quasi-linear FRFs can be obtained from n measured force levels. Therefore, the isolated point must be excluded from subsequent modal analyses. Figure 8 shows the results for the amplitude and phase for the selected measuring channel. However, the process is applied to all sensor positions.

The figure indicates that the FRF with the lowest displacement does not exhibit a distinct maximum. As mentioned earlier in this section, the figure demonstrates the challenges of quasi-linearization based on force-controlled extracted HFS. At the lowest load level, there are numerous closely spaced intersection points (see Fig. 7b). As a result, the force shown in Fig. 7c remains nearly constant in this frequency range. Consequently, the resulting FRF curve for the lowest level is significantly distorted. However, the phase responses show a smooth behavior, especially at higher displacement levels. This aspect is particularly important for modal parameter identification, as it enables the detection of the phase jump at resonance.

Moreover, to enhance the quality of modal model estimation, only measurement channels with a significant ratio between the maximum and average FRF amplitudes within the specified frequency band are retained. This approach is similar to the *mode indicator function* (MIF).[4] As a result, channels without a distinct resonance peak are eliminated, as their pres-

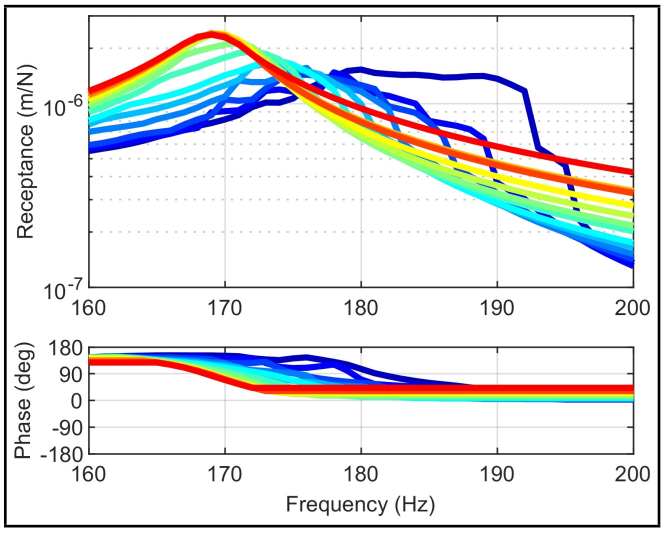

Figure 8. Representation of the derived quasi-linear FRF for all computed constant displacement amplitudes from Fig. 7c at the representative sensor position.

ence can negatively affect the modal identification process.

4.4. Extraction of Modal Parameters

Identifying modal parameters from experimental data often involves numerous manual steps, which can particularly compromise the repeatability of the obtained modal model.[4,46] To address this challenge, a two-step automated modal analysis process has been established. The first step focuses on determining global properties, such as natural frequencies and damping ratios. The second step involves estimating the modal model using a least-squares frequency-domain method. Based on the single nonlinear normal mode theory discussed in Section 2, a combination of global *peak-picking* (PP) to determine natural frequencies and the *half-power method* (HPM) to find damping ratios is considered appropriate.[26] To verify the single degree of freedom (SDoF) assumption, the *complex mode indicator function* (CMIF) is used. This involves performing a singular value decomposition (SVD) of the complex quasi-linearized frequency response function across all frequency points. The squared singular values are then used to calculate the CMIF. The SDoF assumption is valid if only one dominant singular value is present within the resonance range. One key advantage of applying SVD to the quasi-linearized FRF matrix is that it enables accurate identification of natural frequencies via the maximum singular value. This value represents the peak energy across all measurement and reference channels, avoiding misinterpretation arising from sensor placement at local vibration nodes.

Since the CMIF is unsuitable for classical amplitude analyses due to its quadratic nature, and since the distribution of the maximum singular values is generally too broadband for an exact determination of damping, the so-called *enhanced-FRF* (eFRF) or *principal response function* is calculated in the next step.[4,38] To achieve this, the quasi-linearized FRF matrix is scalar-multiplied across the entire frequency band by the singular value vectors $U(f_n)$ and $V(f_n)$ fixed at the resonance point. This mathematical projection serves as an effective spatial filter, minimizing uncorrelated measurement noise and separating the isolated mode's response from the influence of neighboring modes. Another advantage of the eFRF is that it eliminates the need to convert displacements into accelerations. When evaluating receptance, the resonance peaks in the displacement spectrum at high frequencies can be masked by the $1/\omega^2$ decay. Therefore, it may be more appropriate to use accelerance for the peak-picking method, given its horizontal trend. In contrast, the spatial coherence of the redundant measurement data is utilized by decomposing the global FRF matrix through SVD and projecting it onto the eFRF.[4] This approach enables the reliable detection of isolated resonance peaks even with minimal absolute displacement amplitudes. This enhances the analysis process and ensures unit consistency.

The lower f_{lo} and upper f_{up} sideband frequencies are determined by analyzing the magnitude of the eFRF at the half-power points, where the amplitude reaches $1/\sqrt{2}$ of the resonance value. If data is available only on one side of the frequency spectrum, the missing side can be approximated by symmetrically mirroring the observed side.[41] Modal damping is then calculated by evaluating the bandwidth associated with $\Delta f = f_{up} - f_{lo}$.

The measured frequency response functions indicate significant damping in certain resonances. Consequently, an incorrectly estimated damping ratio, often derived under the assumption of weak damping, can lead to an incorrect modal fit. This is particularly problematic in nonlinear cases where the peak can shift to one side. To address this issue, this study uses a multi-criteria evaluation based on empirical best-practice thresholds to differentiate between weak damping $\zeta_{weak} = \Delta f/(2f_n)$ and high damping $\zeta_{high} = (f_{up}^2 - f_{lo}^2)/(4f_n^2)$.[38,41] For this purpose, the relative error between high and low damping ratios is compared: $\Delta\zeta = |\zeta_{high} - \zeta_{weak}|/\max(\zeta_{weak})$. It is assumed that if the difference is below 10 %, and the absolute value of ζ_{weak} is below 5 %, then weak damping is sufficient. Additionally, the Q-factor measures the sharpness of resonance. As a result, Q-values > 30 indicate a narrow resonance peak typical of weakly damped systems. The last criterion focuses on the quality of the HPM. That means the ability to identify both half-power points generally suggests a weakly damped system. If the majority of the criteria indicate weak damping, the modal damping ratio is calculated based on this assumption. This evaluation systematically reduces errors in modal parameter estimation.

The results from the modal parameter identification step are presented in Figs. 9 and 10. To enhance visualization, the eigenfrequencies of the four modes have been normalized to the natural frequency corresponding to the lowest displacement amplitude and plotted as a function of various displacement amplitudes[c].

The illustration shows that all four eigenfrequencies exhibit softening behavior, each changing in a unique nonlinear way. However, all eigenfrequencies converge asymptotically to a certain level. This behavior is characteristic of structures with complex joints and friction contacts.[47] Above a certain excitation level, a shift occurs in these areas from the stick to the slip state, along with a decrease in the damping ratio.

[c]To minimize potential effects based on error propagation when determining mass-normalized modes from modal parameter estimation, the constant displacement amplitudes of the master channel $\mathbf{u}_k$ are used instead of the modal coordinate η_k.

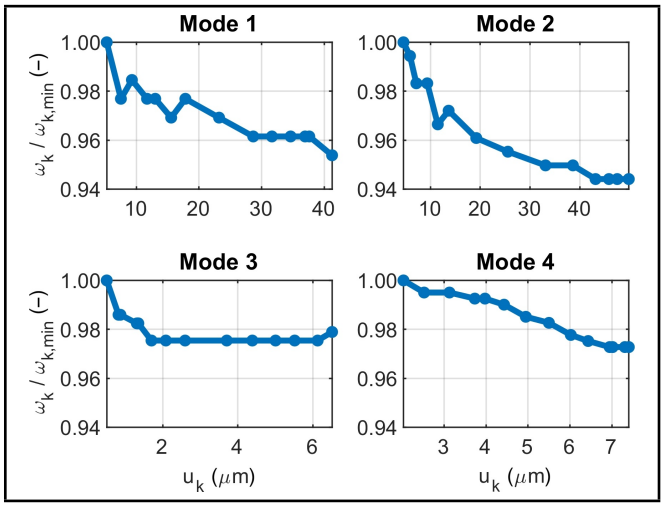

Figure 9. Normalized natural frequencies over the master channel displacement for each mode.

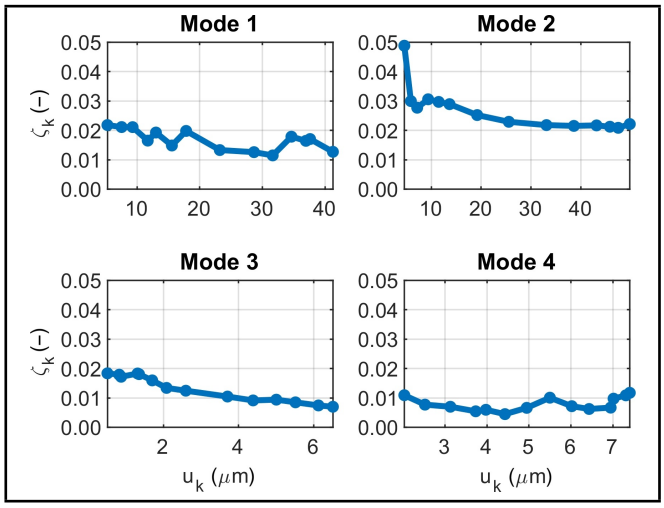

Figure 10. Damping ratio over the master channel displacement for each mode.

An overall decrease trend in damping is observed in Fig. 10, where each mode exhibits distinct modal damping characteristics. Particularly, the second mode illustrates the propagation of errors from the HFS extraction shown in Fig. 8. This leads to a significant overestimation of the damping ratio at the lowest displacement amplitude. Additionally, the damping curve shows considerable variability, indicating that the damping ratio may increase again as the displacement amplitude increases. Increased friction or micro-slip at the contact surfaces of the ball and cylinder bearings with the seat rails may cause an increase in modal damping.[18,30] In contrast, higher preload may reduce modal damping by raising the excitation level.[24] This variability poses challenges for component design, necessitating targeted solutions to effectively influence specific frequencies.

In the second step, a modal model is determined using a least-squares frequency-domain method based on the identified natural frequencies, damping ratios, and poles. As explained in Section 2, the assumption of proportional damping has been made to simplify the presentation of the theoretical concepts. The LSDF method automatically distinguishes between proportional and non-proportional damping. The evaluation is conducted using the *modal phase collinearity* (MPC) criterion. This criterion assesses the complexity of the resulting mode shapes.[4] MPC values greater than 0.80 are nearly purely real and therefore proportionally damped.[48] This detailed analysis of damping requires transforming the classical second-order modal model in Eq. (13) into a first-order system. This transformation is essential because, in systems exhibiting non-proportional damping, the full-rank damping matrix cannot be decoupled using the real eigenvectors of the undamped system described in Eq. (8). As a result, the system must be represented in a state-space format. In this representation, the poles and complex eigenvectors appear in pairs of conjugate complex numbers, facilitating diagonalization in the pole-residue model.

To calculate the MPC values, an initial first-order modal model is implemented during the LSDF process. This model uses a weighted least-squares method to give greater importance to frequency points near the resonance during the identification process.[49,50] This weighting is determined by the amplitudes of the quasi-linear frequency responses, as coherence-based weighting based on statistical averages is not available for stepped-sine measurements.

To ensure a physically accurate representation of the boundary regions, residuals are also determined to compensate for the inertia and stiffness effects of the truncated out-of-band modes.[8] Analogous to the determination of the quasi-linear FRF, the real and imaginary parts of the complex equations are separated using a real-stacking method during the calculation of the lower and upper residuals, thereby preventing phase wrapping. Furthermore, the residuals are fixed at the lowest displacement level because they represent an amplitude-independent linear approximation of the modes outside the investigated frequency range. This aspect is implicitly mentioned in single-nonlinear-mode theory, in which the nonlinearity is isolated to the mode under consideration, while the remaining frequency range is assumed to behave as a linear system.[11,51] The final modal model is established based on the MPC, using either a first- or second-order modal model that incorporates residual terms.

The quality of the modal fit is evaluated using the *modal assurance criterion* (MAC) and the *frequency response assurance criterion* (FRAC).[52] In this context, the MAC analysis is based on unit-maximum-component normalized mode shapes rather than mass normalization.[4] This approach is important because exact mass normalization can lead to errors in non-proportionally damped systems due to the complexity of the modes.[49] The results for the different metrics are illustrated in Fig. 11. To enable a comparison across modes, the x-axis represents a generic displacement level. Each displacement level corresponds to a constant displacement amplitude at the mode-specific master channel, with levels arranged in order of increasing amplitude.

The MPC values exceed 0.8 across all modes and amplitude levels. In combination with the damping values shown in Fig. 11a, it can be concluded that all four modes exhibit weak proportional damping. Notably, the second mode demonstrates a decrease in the MPC value from 1 to 0.90 as the displacement amplitude increases, suggesting increasingly complex natural modes. This indicates a larger relative displacement at the joints, leading to increasingly non-proportional damping.[4,44]

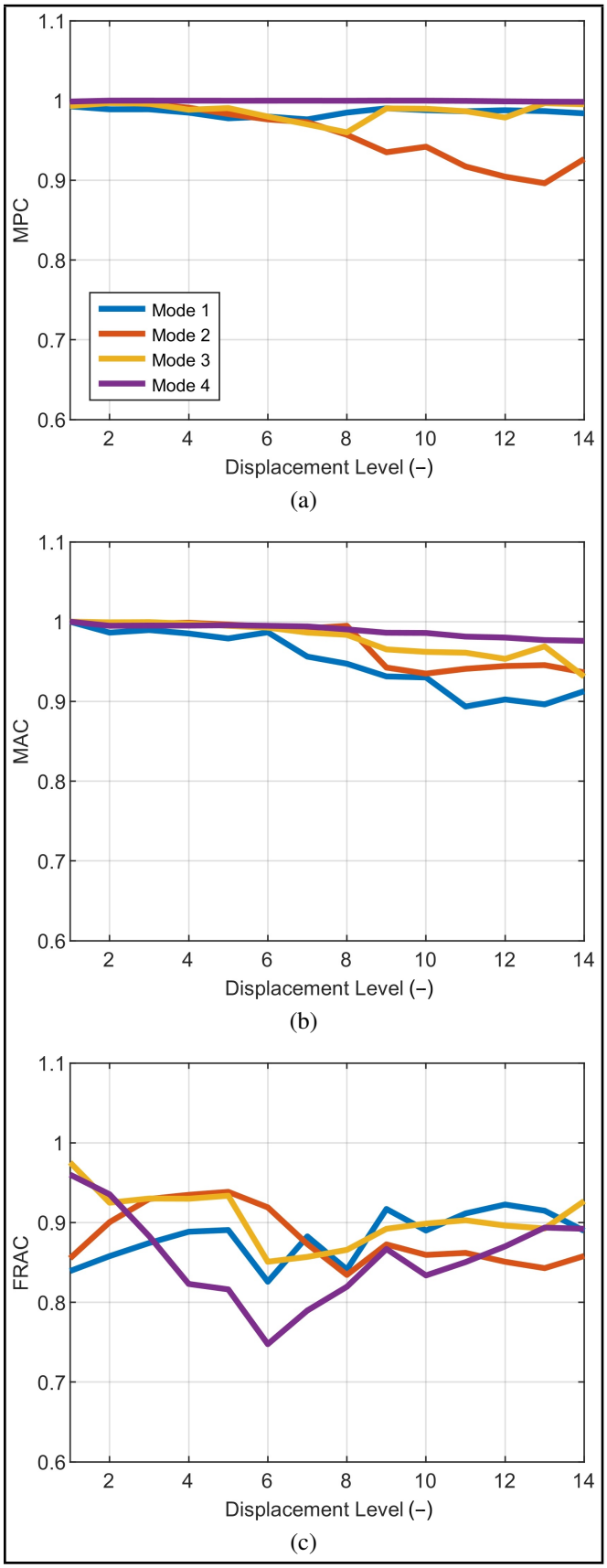

Figure 11. Comparison of various metrics used to evaluate the quality of the modal fit of quasi-linearized frequency response functions across all modes and displacement levels: (a) modal phase collinearity criterion; (b) modal assurance criterion; (c) frequency response assurance criterion.

This observation is consistent with previous findings regarding the decrease in natural frequency and the degree of damping. Therefore, evaluating the MPC criteria is recommended to validate the proportional damping assumption in nonlinear cases.

Additionally, the MAC values in Fig. 11b decrease with increasing load across all four modes. This trend suggests that the structure's spatial deflection becomes progressively distorted by nonlinearity. These observations are consistent with the research conducted by Karaağaçlı et al.[26]

The acceptable FRAC values for the first three modes in Fig. 11c can be attributed to the residual effects of the neighboring modes. In contrast, the FRAC values associated with the fourth mode are notably low. In contrast, the high MPC and MAC values indicate that this mode is least affected by nonlinear effects. Furthermore, it has the largest frequency separation from neighboring modes, making the influence of residuals negligible. The CMIF criterion further confirms that only one mode is present in this range, suggesting that this mode should exhibit the best FRAC values. However, the explanation lies in the very low damping values shown in Fig. 10, which make the FRAC criterion highly sensitive to small errors in identifying the natural frequency and damping. Furthermore, Table 2 clearly indicates that this mode is challenging to identify using the selected master channel. This highlights the significance of choosing an appropriate master channel and the versatile analysis options offered by the presented framework.

5. VALIDATION OF THE IDENTIFIED NONLINEAR MODAL MODEL

In the final step, the modal model discussed in Section 4.4 is validated. To achieve this, the modal parameters are synthesized using the Newton-Raphson method, combined with an arc-length constraint based on the measured force levels. The resulting frequency response functions are then compared with the measured force-controlled FRFs.

To ensure convergence, several extensions to the classical Newton-Raphson method were implemented in this work. First, non-physical values are filtered out, and displacement amplitudes are organized in a way that guarantees strictly monotonic behavior along the x-axis during interpolation[d]. Additionally, shape-preserving piecewise cubic Hermite interpolation polynomials (PCHIP) are utilized to minimize oscillations in the modal parameters. Due to the significant difference in magnitude between the displacement amplitudes (1e-6 m) and the forces (1e1 N), metric weights are introduced to eliminate the dimensions of the quantities, thereby improving the conditioning of the Jacobian matrix. Finally, a step-size controller is employed to prevent divergence at challenging points, such as bifurcations, and to accelerate computations in the linear range. Notably, the combination of the step-size controller and PCHIP splines allows for the incorporation of arbitrary profiles for natural frequencies and damping values. This is particularly important for the damping values shown in

[d]Here, the physical displacement amplitudes of the master channel $\mathbf{u}_r$ are utilized in the Newton solver instead of modal coordinates $\mathbf{q}_r$. Since the mode shape of the master channel Ψ_r represents a fixed scalar, for a given mode, $\Psi_r \approx const.$, the parametrization is equivalent to the substitution $\omega_r(\mathbf{u}_r) = \omega_r(\Psi_r \mathbf{q}_r)$. As long as the sampling points remain monotonic, the PCHIP interpolation yields identical results. Thus, only the x-axis scale changes. The validity of this substitution requires that Ψ_r remain sufficiently constant within the considered amplitude range. This is confirmed by the MAC values from Fig. 11b, which are above 0.8 for all models.

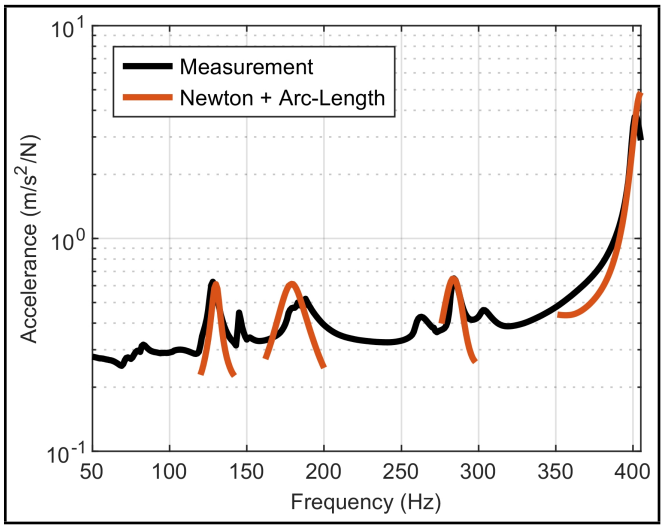

Figure 12. Comparison of the FRF Sum of the Newton synthesis with the measured FRFs at 4 N.

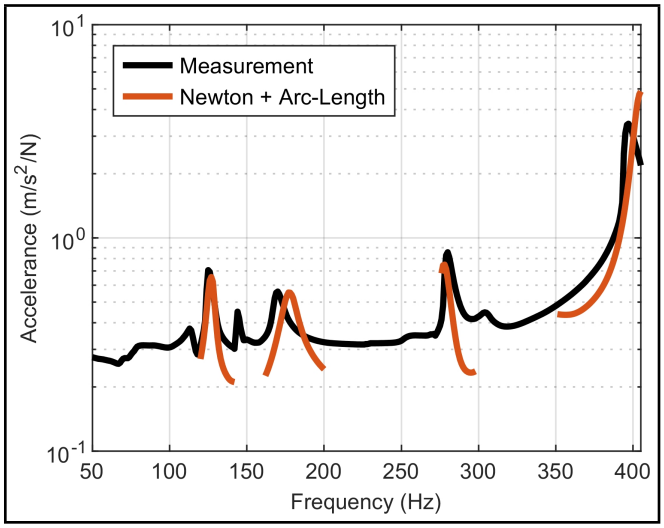

Figure 13. Comparison of the FRF Sum of the Newton synthesis with the measured FRFs at 14 N.

Fig. 10, which exhibit increasing and decreasing trends, suggesting a lack of strict monotonicity. Therefore, even in the absence of bifurcations, the use of the additional arc-length constraint is beneficial to improve the FRF-synthesis quality, instead of using the 1D-Newton-Raphson solver only. Further information regarding the Newton algorithm can be found in references.[35,53–55]

The comparison of the FRF Sum from the Newton synthesis with the measured FRFs is shown in Figs. 12 and 13 for the force levels of 4 N and 14 N, respectively. The results of the Newton synthesis demonstrate good agreement with the measured FRFs across all four modes, particularly at low force levels. However, at higher force levels, the synthesis shows deviations from the measurements for the second and fourth modes.

For the fourth mode, the deviation can be explained by a combination of low modal damping and the selection of a master channel. As a result, the modal parameters fail to represent the actual behavior accurately. Choosing a different measurement channel, such as the front-left channel in the z-direction, which has the best OPD values shown in Table 2, improves agreement, as illustrated in Fig. 14. However, this increases the discrepancy in the second mode. Regarding the

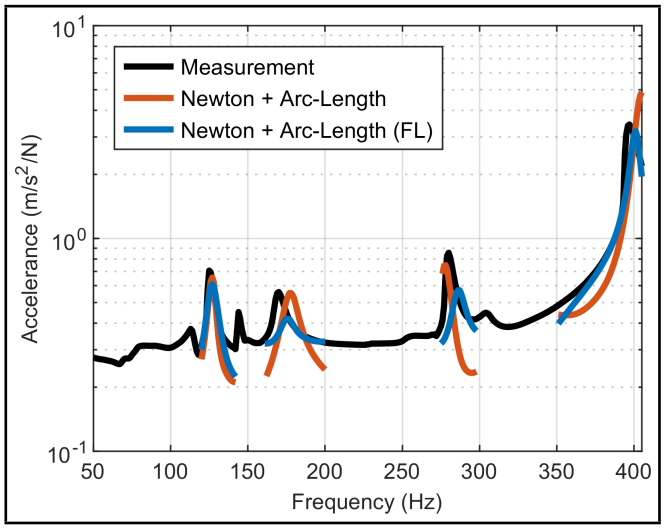

Figure 14. Comparison of the FRF Sum of the Newton synthesis with the measured FRFs at 14 N with the front-left measurement channel in z-direction (FL) as master channel.

second mode, the deviation arises from two factors. First, this mode exhibits the largest frequency shift. Therefore, the separation between the first and second modes is reduced, affecting the SDoF assumption. As a result, the frequency-independent residual terms used in the LSFD process are no longer adequate for approximating the contribution of the first resonance within the frequency band. This results in a partial contribution of the first resonance being incorrectly attributed to the modal parameters of the second mode. Additionally, at higher amplitude levels, the modal model at the boundaries relies on extrapolated values derived from HFS-based forces identification, rather than on physical values. This limitation highlights the challenges of determining quasi-linearized FRFs from force-controlled measurement data.

However, a measurement approach based solely on response displacement control has limitations when applied to thin-walled, lightweight structures with numerous complex contact points, such as the seat rail presented here. The response-controlled method involves significantly larger force amplitudes than force-controlled measurements, leading to displacements in the free-mounting setup and generating strong noise disturbances in the component. Furthermore, the influence of the dynamic shaker mass cannot be entirely neglected. Even though the rail is elastically mounted, it acts as an additional constraint for introducing and measuring the high forces. Consequently, it was not feasible to maintain constant displacements across the entire frequency range that correspond to those determined from the harmonic force surface. Hence, it is advisable to use fixed clamping for lightweight and thin-walled structures to support the generated forces. Additionally, it is essential to ensure adequate distance between the shaker mass and the test object. Thus, RCT measurement is only applicable to a limited extent for thin-walled lightweight structures. Therefore, the method presented in this paper is an efficient approach for determining amplitude-dependent modal parameters of complex nonlinear structures.

6. CONCLUSIONS

A modern vehicle seat structure features various complex adjustment mechanisms and joint assemblies that significantly impact the structural dynamic behavior. Understanding the nonlinear vibration characteristics of these components is essential for optimizing design in terms of noise, vibration, and harshness (NVH) requirements. This study employs an experimental modal analysis and an enhanced harmonic force surface (HFS) approach to examine the nonlinear dynamic behavior of automotive seat rails, which connect the vehicle chassis to the seat structure. This innovative methodology allows for the characterization of amplitude-dependent vibration phenomena in seat rails without requiring prior knowledge of the specific types of nonlinearity involved.

The measurements indicate significant variability in the initial positions after adjusting the upper seat rail. An advanced computer tomography analysis provides detailed insights into the sources of this uncertainty. The imaging identified that a high variation in the ball and cylinder bearings along the lateral position has a substantial impact. The position of the bearings significantly influences the contact areas between the upper and lower rails in a nonlinear fashion, thereby affecting the resulting vibration behavior. Another important advantage of the computer tomography scan is its ability to determine the exact bearing position and the actual subcomponent's material thickness. This type of measurement supports analyses in other contexts, such as the modal updating process of finite element simulations or the optimization process of seat rail designs. The response- and force-controlled stepped-sine test, along with the concept of HFS, addresses measurement uncertainty issues in such applications. This methodology is utilized to analyze the degree of nonlinearity and to calculate the modal parameters.

The experimental investigations demonstrate a weak but distinct nonlinear behavior, characterized by amplitude-dependent decrease in resonance frequencies and variations in modal damping across the investigated modes. Furthermore, the HFS can be established solely through force-controlled tests, as bifurcation phenomena typically associated with nonlinear systems are absent. This significantly reduces the required measurement effort.

The application of the RCT-HFS framework outlined in this paper transforms the force-controlled measurement data within the system, maintaining constant displacements on a selected master channel across the entire frequency range. The resulting quasi-linear FRFs thus represent the same nonlinear state. In this consistent physical form, a combination of peak-picking and half-power methods, along with a least-squares frequency-domain algorithm (LSDF), is used to determine the modal parameters. Finally, the estimated modal parameters have been compared with the measured force-controlled FRFs via FRF synthesis, using the Newton-Raphson method with an integrated arc-length constraint.

The RCT-HFS procedure presented in this work addresses challenges in the three main processing steps. This enables a highly automated implementation of the entire computation process and improves the quality of the estimated modal parameter. The enhancements can be summarized as follows:

1. Determination of quasi-linearized FRFs from the harmonic force surface:
    - Identification of the most suitable master channel based on the optimal driving point (OPD) criterion.
    - Generation of smooth HFSs through polynomial-based Savitzky-Golay filtering of the master channel.
    - Reduction of measurement noise in the displacement spectra using the measured transfer functions.
2. Modal parameter estimation using peak-picking and LSDF:
    - Extrapolation of the boundaries of the quasi-linear FRF to ensure the determination of the modal model, particularly for larger displacement amplitudes.
    - Evaluation of the SDoF assumption using the complex mode indicator function (CMIF).
    - Determination of natural frequencies based on the enhanced FRF approach.
    - Distinction between weak and strong damping via multi-criteria evaluation for precise determination of damping.
    - Distinguishing between proportional and non-proportional damping based on the modal phase collinearity (MPC) criterion.
    - Determination of out-of-band residuals using the least-squares method.
    - Evaluation of the quality of the modal model using the modal assurance (MAC) and frequency response assurance criterion (FRAC).
3. FRF synthesis using Newton-Raphson:
    - Improvement of the conditioning of the Jacobi matrix via metric weighting of the displacements and forces.
    - Enabling arbitrary frequency and damping behavior using piecewise cubic Hermite integration polynomials and a step-size controller.

These enhancements to the RCT-HFS framework enable a comprehensive analysis of the vehicle seat rail's nonlinear behavior. Therefore, the four modes examined exhibit weak proportional damping characteristics. Notably, the second mode, which shows the greatest frequency shift, reveals increasing non-proportional damping as the displacement amplitude increases. This indicates an increasing sliding in the contact areas and is supported by decreases in the natural frequency and the damping ratio. However, it is important to note that each mode has its own behavior, in which the damping ratio tends to increase in some modes as the displacement amplitude increases.

Additionally, the MAC values decrease with increasing load levels, indicating that the modes become increasingly distorted by nonlinearities. It was also found that the FRAC values, along with the Newton synthesis of the 2nd and 4th modes,

did not yield optimal results. In the 4th mode, this can be explained by a combination of very low damping ratios, which make the FRAC criterion sensitive to even minor inaccuracies in determining modal parameters, and the choice of the master channel. The second mode violates the single-degree-of-freedom assumption at higher displacement amplitudes. This results in the influence of the first mode increasingly appearing in the residuals of the second mode. Moreover, the extrapolated boundary values of the forces from the harmonic force surface become less representative of the physical behavior as displacement increases, highlighting a limitation of the RCT-HFS approach. In this context, further methodological limitations are investigated. Therefore, the foundation of the RCT-HFS concept presents significant limitations. Extracting physical values from a geometric shape is highly sensitive to disturbances that can affect its contour. Consequently, these effects can be summarized as follows:

- In this context, selecting an appropriate master channel is crucial. However, it has been demonstrated that, even with the OPD criterion, not all modes can be adequately described by a single master channel.
- Moreover, the degree of dependence on the number of measurements is significant. Insufficient sample points can result in insufficient data for interpolating the harmonic force surface. Conversely, having too many sample points can result in very similar displacement amplitudes, causing broad peaks in the quasi-linearized FRFs, particularly at low amplitudes, which are essential for the out-of-band residuals. To achieve the highest possible resolution without broadening the FRF peaks, a global smoothing of the HFS using Gaussian process regression (GPR) after local filtering of the master channel could be beneficial.
- Furthermore, additional analyses are necessary to accurately classify isolas and prevent misclassification as geometric artifacts caused by the intersection planes. The method also assumes that the system's first harmonic is dominant. However, in highly nonlinear systems, dominant higher harmonics may appear, necessitating further verification of this assumption.
- The force-controlled measurement method is strictly limited to the immediate frequency range of the resonance. This is essential for ensuring good mode separation and remaining within the range of physical values as proposed by the force extrapolation method.

A main benefit of the presented approach is the ability to analyze nonlinear systems without prior knowledge of the type of nonlinearity. This characteristic is especially valuable at the beginning of the system identification process, as it helps develop a general understanding of the nonlinear behavior. Typically, force-controlled measurement is the starting point for linear and nonlinear experimental modal analysis. In this context, the proposed framework can be used to determine appropriate initial values for displacement-controlled measurements and more advanced nonlinear analysis. Additionally, it allows the characterization of an optimal master channel and the evaluation of SDoF and damping assumptions within a single integrated process.

This research quantifies the nonlinear dynamic characteristics of automotive seat rails to enhance NVH design and reduce analysis time. The findings offer valuable insights into the complex structural dynamics of seat rails and the HFS methodology. Additionally, the study provides a practical framework for conducting nonlinear experimental modal analysis, highlighting the advantages and limitations of the approaches and thereby facilitating a more targeted application of these methods. However, further research is needed to improve HFS modeling and the accuracy of force identification. Furthermore, the presented framework should be extended to systems exhibiting greater nonlinearity.

REFERENCES

[1] Mazur, M., Leary, M., Sunan, H., Baxter, T., and Subic, A. Benchmarking study of automotive seat track sensitivity to manufacturing variation, *Proceedings of the 18th International Conference on Engineering Design ICED11*, **10**, 402–412, (2011).

[2] Yu, H., Zhang, X., and Zhang, C. Optimization method of the car seat rail abnormal noise problem based on the finite element method, *Shock and Vibration*, **17**, 1–13, (2017). https://doi.org/10.1155/2017/4132092

[3] Zhang, Z., Jin, K., Li, F., Lu, C., Chai, G., and Ye, D. Effects of adjustment devices on the fore-and-aft mode of an automobile seat system: headrest, height adjuster, recliner and track slide, *Proceedings of the Institution of Mechanical Engineers, Part D: Journal of Automobile Engineering*, **230** (8), 1140–1152, (2016). https://doi.org/10.1177/0954407015602823

[4] Allemang, R. J. and Avitabile, P., Eds. *Handbook of Experimental Structural Dynamics*. New York, NY, USA: Springer New York, (2022).

[5] Lin, R. M., Mottershead, J. E., and Ng, T. Y. A state-of-the-art review on theory and engineering applications of eigenvalue and eigenvector derivatives, *Mechanical Systems and Signal Processing*, **138**, 1–32, (2020). https://doi.org/10.1016/j.ymssp.2019.106536

[6] Brake, M. R., Ed. *The Mechanics of Jointed Structures: Recent research and open challenges for developing predictive models for structural dynamics*. Cham, Switzerland: Springer International Publishing, (2018).

[7] Islam, M. M., Mäder, M., Lehmann, R., and Marburg, S. Experimental modal analysis of stators analyzing the effects of lamination and winding, *Journal of Vibration and Acoustics*, **145** (5), 1–8, (2023). https://doi.org/10.1115/1.4062839

[8] Nestorović, T., Trajkov, M., and Patalong, M. Identification of modal parameters for complex structures by experimental modal analysis approach, *Advances in Mechanical Engineering*, **8** (5), 1–16, (2016). https://doi.org/10.1177/1687814016649110

[9] Rosenberg, R. M. Normal modes of nonlinear dual-mode systems, *Journal of Applied Mechanics*, **27** (2), 263–268, (1960). https://doi.org/10.1115/1.3643948

[10] Kerschen, G., Worden, K., Vakakis, A. F., and Golinval, J.-C. Past, present and future of nonlinear system identification in structural dynamics, *Mechanical Systems and Signal Processing*, **20** (3), 505–592, (2006). https://doi.org/10.1016/j.ymssp.2005.04.008

[11] Kerschen, G., Peeters, M., Golinval, J.-C., and Vakakis, A. F. Nonlinear normal modes, Part I: A useful framework for the structural dynamicist, *Mechanical Systems and Signal Processing*, **23** (1), 170–194, (2009). https://doi.org/10.1016/j.ymssp.2008.04.002

[12] Noël, J. P. and Kerschen, G. Nonlinear system identification in structural dynamics: 10 more years of progress, *Mechanical Systems and Signal Processing*, **83**, 2–35, (2017). https://doi.org/10.1016/j.ymssp.2016.07.020

[13] Gonçalves, P. B. Nonlinear normal modes and reduced order models, *Lectures on Nonlinear Dynamics*, ser. Understanding Complex Systems, Castilho Piqueira, J. R., Nigro Mazzilli, C. E., Pesce, C. P., and Franzini, G. R., Eds., 105–132. Cham, Switzerland: Springer Nature Switzerland, (2024).

[14] Castilho Piqueira, J. R., Nigro Mazzilli, C. E., Pesce, C. P., and Franzini, G. R., Eds. *Lectures on Nonlinear Dynamics*, ser. Understanding Complex Systems. Cham, Switzerland: Springer Nature Switzerland, (2024).

[15] Szemplińska-Stupnicka, W. The modified single mode method in the investigations of the resonant vibrations of non-linear systems, *Journal of Sound and Vibration*, **63** (4), 475–489, (1979). https://doi.org/10.1016/0022-460X(79)90823-X

[16] Peeters, B., El-Kafafy, M., and Guillaume, P. The new PolyMAX Plus method: Confident modal parameter estimation even in very noisy cases, *Proceedings of ISMA 2012 International Conference on Noise and Vibration Engineering*, 2801–2814, (2012).

[17] Gibert, C. Fitting measured frequency response using non-linear modes, *Mechanical Systems and Signal Processing*, **17** (1), 211–218, (2003). https://doi.org/10.1006/mssp.2002.1562

[18] Ehrhardt, D. A. and Allen, M. S. Measurement of nonlinear normal modes using multi-harmonic stepped force appropriation and free decay, *Mechanical Systems and Signal Processing*, 76-77, 612–633, (2016). https://doi.org/10.1016/j.ymssp.2016.02.063

[19] Kwarta, M., and Allen, M. S. Nonlinear normal mode backbone estimation with near-resonant steady state inputs, *Mechanical Systems and Signal Processing*, **162**, 1–24, (2022). https://doi.org/10.1016/j.ymssp.2021.108046

[20] Scheel, M., Weigele, T., and Krack, M. Challenging an experimental nonlinear modal analysis method with a new strongly friction-damped structure, *Journal of Sound and Vibration*, **485**, 115580, (2020). https://doi.org/10.1016/j.jsv.2020.115580

[21] Scheel, M. Nonlinear modal testing of damped structures: Velocity feedback vs. phase resonance, *Mechanical Systems and Signal Processing*, **165**, 1–19, (2022). https://doi.org/10.1016/j.ymssp.2021.108305

[22] Kuran, B. and Özgüven, H. N. A modal superposition method for non-linear structures, *Journal of Sound and Vibration*, **189** (3), 315–339, (1996). https://doi.org/10.1006/jsvi.1996.0022

[23] Arslan, Ö., Aykan, M., and Özgüven, H. N. Parametric identification of structural nonlinearities from measured frequency response data, *Mechanical Systems and Signal Processing*, **25** (4), 1112–1125, (2011). https://doi.org/10.1016/j.ymssp.2010.10.010

[24] Karaağaçlı, T., and Özgüven, H. N. Experimental modal analysis of nonlinear systems by using response-controlled stepped-sine testing, *Mechanical Systems and Signal Processing*, **146**, 1–24, (2021). https://doi.org/10.1016/j.ymssp.2020.107023

[25] Karaağaçlı, T., and Özgüven, H. N. Experimental quantification and validation of modal properties of geometrically nonlinear structures by using response-controlled stepped-sine testing, *Experimental Mechanics*, **62** (2), 199–211, (2022). https://doi.org/10.1007/s11340-021-00784-9

[26] Karaağaçlı, T., and Çelik, F. K. Modal analysis of non-conservative systems with friction-induced strong nonlinear damping by using response-controlled testing, *Mechanical Systems and Signal Processing*, **221**, 111718, (2024). https://doi.org/10.1016/j.ymssp.2024.111718

[27] Karaağaçlı, T., and Özgüven, H. N. European Patent EP4078113: A novel experimental modal analysis method based on response control approach for nonlinear engineering structures, (2024).

[28] Karaağaçlı, T., and Özgüven, H. N. A frequency domain nonparametric identification method for nonlinear structures: Describing surface method, *Mechanical Systems and Signal Processing*, **144**, 1–23, (2020). https://doi.org/10.1016/j.ymssp.2020.106872

[29] Koyuncu, A., Karaağaçlı, T., Şahin, M., and Özgüven, H. N. Experimental modal analysis of nonlinear amplified piezoelectric actuators by using response-controlled stepped-sine testing, *Experimental Mechanics*, **62** (9), 1579–1594, (2022). https://doi.org/10.1007/s11340-022-00878-y

[30] Gürbüz, M. F., Karaağaçlı, T., Özer, M. B., and Özgüven, H. N. Bypassing the repeatability issue in nonlinear experimental modal analysis of jointed structures by using the RCT-HFS framework, *Nonlinear Structures & Systems, Volume 1*, ser. Conference Proceedings of the Society for Experimental Mechanics Series, Brake, M. R., Renson, L., Kuether, R. J., and Tiso, P., Eds., 75–80. Cham, Switzerland: Springer Nature Switzerland, (2024).

[31] Nayfeh, A. H. and Mook, D. T. *Nonlinear Oscillations*. Wiley, (1995).

[32] Marburg, S. Normal modes in external acoustics. Part I: Investigation of the one-dimensional duct problem, *Acta Acustica united with Acustica*, **91** (6), 1063–1078, (2005).

[33] Tanrikulu, O., Kuran, B., Özgüven, H. N., and Imregun, M. Forced harmonic response analysis of nonlinear structures using describing functions, *AIAA Journal*, **31** (7), 1313–1320, (1993). https://doi.org/10.2514/3.11769

[34] Kalaycıoğlu, T. and Özgüven, H. N. Nonlinear structural modification and nonlinear coupling, *Mechanical Systems and Signal Processing*, **46** (2), 289–306, (2014). https://doi.org/10.1016/j.ymssp.2014.01.016

[35] Setio, S., Setio, H. D., and Jezequel, L. A method of nonlinear modal identification from frequency response tests, *Journal of Sound and Vibration*, **158** (3), 497–515, (1992). https://doi.org/10.1016/0022-460X(92)90421-S

[36] Ferhatoglu, E., Cigeroglu, E., and Özgüven, H. N. A novel modal superposition method with response dependent nonlinear modes for periodic vibration analysis of large MDOF nonlinear systems, *Mechanical Systems and Signal Processing*, **135**, 1–20, (2020). https://doi.org/10.1016/j.ymssp.2019.106388

[37] Yunus, M. A., Bahari, A. R., Rani, M. N. A., Yahya, Z., and Rahim, M. A. Reliability of response-controlled stepped sine testing for experimental detection of nonlinear structure, *International Journal of Automotive and Mechanical Engineering*, **20** (3), 10618–10625, (2023). https://doi.org/10.15282/ijame.20.3.2023.05.0819

[38] Ewins, D. J. *Modal Testing: Theory, Practice and Application*, 2nd ed., ser. Mechanical engineering research studies Engineering dynamics series. Baldock: Research Studies Press, (2009). [Online]. Available: http://www.loc.gov/catdir/enhancements/fy0745/97043590-d.html

[39] Pasch, G., Wischmann, S., Drichel, P., Jacobs, G., and Berroth, J. Enhanced method for optimum driving point identification for modal testing, *Journal of Vibration and Control*, **29** (7–8), 1472–1483, (2023). https://doi.org/10.1177/10775463211064699

[40] Schafer, R. What is a Savitzky-Golay filter? [Lecture notes], *IEEE Signal Processing Magazine*, **28** (4), 111–117, (2011). https://doi.org/10.1109/MSP.2011.941097

[41] He, J. and Fu, Z.-F. *Modal Analysis*, 1st ed. Oxford, UK: Elsevier, (2001).

[42] Krack, M. Nonlinear modal analysis of nonconservative systems: Extension of the periodic motion concept, *Computers & Structures*, **154**, 59–71, (2015). https://doi.org/10.1016/j.compstruc.2015.03.008

[43] Kerschen, G. and Vakakis, A. F. Modal analysis of nonlinear mechanical systems, *Handbook of Experimental Structural Dynamics*, Allemang, R. J. and Avitabile, P., Eds., 799–830. New York, NY, USA: Springer New York, (2022).

[44] Brake, M. R., Renson, L., Kuether, R. J., and Tiso, P., Eds. *Nonlinear Structures & Systems, Volume 1*. Cham, Switzerland: Springer International Publishing, (2023).

[45] Anastasio, D., Marchesiello, S., and Kerschen, G. Estimation of the periodic solutions of geometrically nonlinear structures by broadband excitation, *Proceedings of ISMA 2024 International Conference on Noise and Vibration Engineering*, 2138–2150, (2024).

[46] Verboven, P. *Frequency-Domain System Identification for Modal Analysis*, PhD thesis, Vrije Universiteit Brussel, Brussels, Belgium, (2002).

[47] Laxalde, D. and Thouverez, F. Complex non-linear modal analysis for mechanical systems: Application to turbomachinery bladings with friction interfaces, *Journal of Sound and Vibration*, **322** (4–5), 1009–1025, (2009). https://doi.org/10.1016/j.jsv.2008.11.044

[48] Koruk, H. and Sanliturk, K. Y. A novel definition for quantification of mode shape complexity, *Journal of Sound and Vibration*, **332** (14), 3390–3403, (2013). https://doi.org/10.1016/j.jsv.2013.01.039

[49] Böswald, M., Göge, D., UFuüllekrug, U., and Govers, Y. A review of experimental modal analysis methods with respect to their applicability to test data of large aircraft structures, *Proceedings of ISMA 2006 International Conference on Noise and Vibration Engineering*, 2461–2482, (2006).

[50] Amador, S., El-Kafafy, M., Cunha, Á., and Brincker, R. A new maximum likelihood estimator formulated in pole-residue modal model, *Applied Sciences*, **9** (15), 3120, (2019). https://doi.org/10.3390/app9153120

[51] Peeters, M., Kerschen, G., and Golinval, J. C. Dynamic testing of nonlinear vibrating structures using nonlinear normal modes, *Journal of Sound and Vibration*, **330** (3), 486–489, (2011). https://doi.org/10.1016/j.jsv.2010.08.028

[52] Lee, D., Ahn, T.-S., and Kim, H.-S. A metric on the similarity between two frequency response functions, *Journal of Sound and Vibration*, **436**, 32–45, (2018). https://doi.org/10.1016/j.jsv.2018.08.051

[53] Crisfield, M. A. A fast incremental/iterative solution procedure that handles "snap-through", *Computers & Structures*, **13** (1–3), 55–62, (1981). https://doi.org/10.1016/0045-7949(81)90108-5

[54] Ritto-Corrêa, M. and Camotim, D. On the arc-length and other quadratic control methods: Established, less known and new implementation procedures, *Computers & Structures*, **86** (11–12), 1353–1368, (2008). https://doi.org/10.1016/j.compstruc.2007.08.003

[55] Hiermeier, M. *Advanced Non-Linear Solution Techniques for Computational Contact Mechanics*, PhD thesis, Technical University of Munich, Munich, Germany, (2020).